TSINGHUA SCIENCE AND TECHNOLOGY
ISSN 1007-0214 08/13 pp 303–314
DOI: 10.26599 / TST.2018.9010001
Volume 23, Number 3, June 2018

Novel Model Using Kernel Function and Local Intensity Information for Noise Image Segmentation

Gang Li, Haifang Li, and Ling Zhang*

Abstract: It remains a challenging task to segment images that are distorted by noise and intensity inhomogeneity. To overcome these problems, in this paper, we present a novel region-based active contour model based on local intensity information and a kernel metric. By introducing intensity information about the local region, the proposed model can accurately segment images with intensity inhomogeneity. To enhance the model's robustness to noise and outliers, we introduce a kernel metric as its objective functional. To more accurately detect boundaries, we apply convex optimization to this new model, which uses a weighted total-variation norm given by an edge indicator function. Lastly, we use the split Bregman iteration method to obtain the numerical solution. We conducted an extensive series of experiments on both synthetic and real images to evaluate our proposed method, and the results demonstrate significant improvements in terms of efficiency and accuracy, compared with the performance of currently popular methods.

Key words: kernel metric; image segmentation; local intensity information; convex optimization

1 Introduction

Image segmentation is a worthy and important problem in computer vision and image processing, for which researchers have proposed many algorithms for image segmentation based on various theories[1, 2]. Due to their solid foundations, the models based on evolution curves and geometric active contours are widely used.

With respect to energy functions that use different image information, these models can generally be divided into two categories: edge-based[3–7] and region-based[8–15]. Edge-based models, which utilize changing gradient information to guide the evolving curve to object boundaries, exhibit good performance when the image segments have strong edges, but fail to detect objects with weak boundaries. In addition, they are sensitive to image noise. Region-based models mainly utilize region descriptors (such as the mean, variance, etc.) to construct the fitting term. Unlike edge-based models, they do not rely on image gradients but exploit statistical information about image regions, so they can segment objects with weak boundaries and are less sensitive to noise.

One of the most famous region-based models (active contour without edges) is the CV model[9] proposed by Chan and Vese, which is a unique model using Mumford-Shah segmentation[8] model. This model is based on the assumption that the distribution of gray values within each image sub-region is uniform, and its energy functional is established based on the difference between each pixel and the regional average. However, this model cannot obtain accurate segmentation results for some images that are corrupted by non-uniform intensity and noise.

To deal with the above problems and overcome intensity inhomogeneity, Li et al. proposed a Region-Scalable Fitting (RSF) model[10] that utilizes local region information as a constraint in spatially varying local

• Gang Li, Haifang Li, and Ling Zhang are with College of Computer Science and Technology, Taiyuan University of Technology, Taiyuan 030024, China. E-mail: ligang@tyut.edu.cn; lihaifang@tyut.edu.cn; zl2090@126.com.

* To whom correspondence should be addressed.
Manuscript received: 2017-07-17; revised: 2017-08-20; accepted: 2017-09-01

regions. However, the RSF model requires four convolution calculations, which means it has high computational complexity. Zhang et al. also used local information to construct a local image fitting energy[11]. Their model achieves similar results to those of the RSF model with less computational cost. The Local Intensity Clustering (LIC) model[12], proposed by Li et al., derives an LIC property of image intensities. However, by using only the intensity means as its classification standard, this method may not be able to accurately extract object boundaries. Wang et al. employed Gaussian distributions to model the local Gaussian fitting energy[13], which overcomes the difficulties presented by intensity inhomogeneity. However, since means and variances are spatially varying functions, the computation in this method is also expensive. Apart from cost, these models are also sensitive to the location of the initial contours to some extent and cannot obtain better results for images with high noise levels. Recently, Xie et al. proposed a Robust Level Set Method (RLSM)[15] that exploits the difference between local statistical information and global information to suppress high noise levels. However, the evolution of the curve is unstable where the local intensity information is similar to the global information, so the RLSM model does not achieve satisfactory results for images with varying high noise levels. In addition, the above models base their measurements on the Euclidean distance, so the segmentation results are susceptible to noise.

To overcome the limitations of the CV model, which fails to detect objects with intensity inhomogeneity and has a slow processing speed, in this paper, we introduce local image information into the CV model, based on the assumption of a piecewise constant. We also use a kernel function metric to construct a robust non-Euclidean distance measurement, whereby the evolution of the contour can overcome the impacts of inhomogeneity and noise on the segmentation results. Moreover, we utilize the global optimization method to obtain a global convex segmentation model, which overcomes the impact of initialization on the segmentation results. Lastly, to increase computational efficiency, we use the split Bregman method to realize a fast solution.

The remainder of this paper is organized as follows: In Section 2, we briefly describe the Chan-Vese model and the kernel theory. In Section 3, we describe our model and its numerical method. In Section 4, we validate our proposed method in a series of experiments on synthetic and real images and compare our results with those of various other methods. We present our conclusions in Section 5.

2 Previous Work

2.1 Chan-Vese model

Chan and Vese proposed their model[9] based on the assumption that an image is composed of two parts of constant intensity, in which the energy functional is defined as follows:

$$E^{cv}(c_1,c_2,C)=\lambda_1\int_{inside(C)}(I(x,y)-c_1)^2\mathrm{d}x\mathrm{d}y+\lambda_2\int_{outside(C)}(I(x,y)-c_2)^2\mathrm{d}x\mathrm{d}y+\upsilon\cdot length(C) \quad (1)$$

Let C be a closed active contour in the image domain Ω, which separates image I into two regions: the target region $\Omega_C = inside(C)$ and the background region $\Omega \setminus \Omega_C = outside(C)$, where λ_1, λ_2, and υ are nonnegative constants, c_1 and c_2 represent the intensity averages of regions *inside*(C) or *outside*(C). The first and second terms are data terms that guide the evolution curve to the desired object boundary. The last term is the length of curve C, which smooths the contour.

We introduce the level set function $\phi(x,y)$ to minimize the energy functional, as follows:

$$\begin{cases}\phi(x,y)>0, & (x,y)\in\Omega_C,\\ \phi(x,y)=0, & (x,y)\in C,\\ \phi(x,y)<0, & (x,y)\in\Omega\setminus\Omega_C\end{cases} \quad (2)$$

With a level set representation, the energy functional can be written as follows:

$$E^{cv}(c_1,c_2,\phi)=\lambda_1\int_{\Omega}(I(x,y)-c_1)^2H(\phi(x,y))\mathrm{d}x\mathrm{d}y+\lambda_2\int_{\Omega}(I(x,y)-c_2)^2(1-H(\phi(x,y))\mathrm{d}x\mathrm{d}y+\upsilon\cdot\int_{\Omega}\delta(\phi(x,y))|\nabla\phi(x,y)|\mathrm{d}x\mathrm{d}y \quad (3)$$

where $H(\phi)$ and $\delta(\phi)$ represent the Heaviside and Dirac functions, respectively. Using a variational method, we derive the function as follows:

$$\frac{\partial\phi}{\partial t}=\delta(\phi)\left[-\lambda_1(I(x,y)-c_1)^2+\lambda_2(I(x,y)-c_2)^2+\upsilon div\left(\frac{\nabla\phi}{|\nabla\phi|}\right)\right] \quad (4)$$

where c_1 and c_2 are defined as follows:

$$c_1(\phi)=\frac{\int_\Omega I(x)H(\phi(x))\mathrm{d}x}{\int_\Omega H(\phi(x))\mathrm{d}x} \tag{5}$$

$$c_2(\phi)=\frac{\int_\Omega I(x)(1-H(\phi(x)))\mathrm{d}x}{\int_\Omega (1-H(\phi(x)))\mathrm{d}x} \tag{6}$$

The CV model utilizes region information to segment images, but cannot effectively segment images with weak edges. Furthermore, this model does not consider the local region information in the image, so it cannot accurately deal with images with complex backgrounds and non-homogeneities. Also, since the CV model uses the Euclidean distance to measure the distance between the pixel and the fitting center, which ignores differences between noisy and normal pixels, all pixels are given the same weight in the calculation. Therefore, the distance measurement cannot accurately segment images with intensity inhomogeneity.

2.2 Kernel theory

Using a nonlinear mapping function to map n-dimensional feature vectors into a high-dimensional space H, we can construct a new classification function to achieve classification. Following Mercer's theorem[16], we can represent the inner product of the high-dimensional space by a kernel function, as follows:

$$K(x,y)=\langle \Phi(x),\Phi(y)\rangle=\Phi(x)^{\intercal}\Phi(y) \tag{7}$$

The Gaussian radial-basis function is a frequently used kernel function, which is defined as follows:

$$K(x,y)=\exp\left(-\frac{\|x-y\|^2}{\sigma_k^2}\right) \tag{8}$$

The kernel function metric between vectors x and y can be represented as follows:

$$\begin{aligned}&\|\Phi(x)-\Phi(y)\|^2=(\Phi(x)-\Phi(y))(\Phi(x)-\Phi(y))^{\intercal}=\\&\Phi(x)\Phi(x)^{\intercal}-2\Phi(x)\Phi(y)^{\intercal}+\Phi(y)\Phi(y)^{\intercal}=\\&K(x,x)-2K(x,y)+K(y,y)\end{aligned} \tag{9}$$

where $K(x,x)=K(y,y)=1$. Thus, we can simplify the kernel metric as follows:

$$\|\Phi(x)-\Phi(y)\|^2=2(1-K(x,y)) \tag{10}$$

The introduction of the kernel functions makes the new classification function linearly separable in high-dimensional space, and improves the accuracy of the measurement. The inner product in the high-dimensional feature space can be realized implicitly by the kernel function in the input space, without increasing the complexity of the algorithm.

3 Proposed Model

3.1 Local piecewise model based on kernel function

To overcome the influence of high noise levels and intensity inhomogeneity on the segment results, we propose a novel active contour model based on a kernel function and local intensity information. For a given pixel $x\in\Omega$, we consider x to be the center point, and ρ the radius of the circular neighborhood $O_x\triangleq y:|x-y|<\rho$. Assuming that an image consists of a disjointed sub-region $\{\Omega_i\}_{i=1}^N$ and satisfies the following relationship: $\Omega=\bigcup_{i=1}^N$, $\Omega_i\bigcap\Omega_j=\varnothing$, $i\neq j$, for each pixel $x\in\Omega_i$, we can define the local energy as follows:

$$E_x^i=\int G_\sigma(x-y)\|\Phi(I(y))-\Phi(c_i)\|^2\mathrm{d}y \tag{11}$$

where $I(y)$ is the intensity value of point y in neighborhood O_x, the size of the neighborhood O_x is controlled by the Gaussian function G_σ, and the constant c_i is the average intensity in the sub-region Ω_i. The local energy is defined based on the kernel function metric of the intensities of all points within its neighborhood and the average intensity of the region. We can define a truncated Gaussian function, as follows:

$$G_\sigma=\begin{cases}\frac{1}{\sqrt{2\pi}\sigma}\exp\left(\frac{|u|^2}{2\sigma^2}\right),\ |u|\leqslant\rho;\\0\end{cases} \tag{12}$$

where σ is the standard deviation of the Gaussian function, such that $\int G(x-y)=1$ for $x\in O_x$, and ρ is the radius of neighborhood O_x. We consider that there is a certain correlation between the intensity of point x and other points in neighborhood O_x. With $G(x-y)$ as the weight assigned to the values $\|\Phi(I(y))-\Phi(c_i)\|^2$, the contribution of intensity $I(y)$ near the center point x gives greater weight to energy E_x^i. To obtain the target boundary over the entire domain, we must find a closed contour C that minimizes the local energy for all x in image domain Ω. We define an energy function for the integral of E_x^i over all the center points x in image domain Ω. Therefore, we can define the following energy functional:

$$E=\sum_{i=1}^N\int_{\Omega_i}E_i^x\mathrm{d}x \tag{13}$$

With the E_i^x value in Eq. (11), we can rewrite the

energy functional as follows:

$$E(c_1,c_2,C)=\sum_{i=1}^{N}\int_{\Omega_i}(\int G_\sigma(x-y)\|\Phi(I(y))-\Phi(c_i)\|^2\mathrm{d}y)\mathrm{d}x \tag{14}$$

3.2 Numerical implementation of the model

We consider a two-phase case in which the image domain is segmented into two disjointed regions, Ω_1 and Ω_2. In this case, regions Ω_1 and Ω_2 can be represented with their membership functions defined by $M_1(\phi)=H(\phi)$ and $M_2(\phi)=1-H(\phi)$, respectively. We then convert them to a level set formulation to solve the energy minimization problem, and rewrite the energy functional in Eq. (14) as shown below:

$$E(c_1,c_2,\phi)=\sum_{i=1}^{N}\int(\int G_\sigma(x-y)\|\Phi(I(y))-\Phi(c_i)\|^2\mathrm{d}yM_i(\phi(x)))\mathrm{d}x \tag{15}$$

For convenience, we represent the constants c_1 and c_2 with the vector $c=(c_1,c_2)$, and can thus rewrite the energy as follows:

$$E(c_1,c_2,\phi)=\sum_{i=1}^{N}\int e_i(x)M_i(\phi(x))\mathrm{d}x \tag{16}$$

where e_i is a function defined by the following:

$$e_i=\int G_\sigma(x-y)\|\Phi(I(y))-\Phi(c_i)\|^2\mathrm{d}y,\quad i=1,2 \tag{17}$$

By Eq. (10), we can simplify this function as follows:

$$e_i=\int G_\sigma(x-y)(1-K(I(y),c_i))\mathrm{d}y,\quad i=1,2 \tag{18}$$

Then, we can write the entire objective energy function for the image segmentation, as follows:

$$E(c_1,c_2,\phi)=\sum_{i=1}^{N}\int e_i(x)M_i(\phi(x))\mathrm{d}x+\upsilon\cdot\int_\Omega\delta(\phi(x))|\nabla\phi(x)|\mathrm{d}x \tag{19}$$

where the second term is a length term that smooths the contour by penalizing its length. By the calculus of variations, while keeping c_1, c_2 fixed and minimizing the energy functional with respect to ϕ, we can derive the following gradient descent flow:

$$\frac{\partial\phi}{\partial t}=-\delta_\varepsilon(\phi)(e_1-e_2)+\upsilon\delta_\varepsilon(\phi)div\left(\frac{\nabla\phi}{|\nabla\phi|}\right) \tag{20}$$

where e_1 and e_2 are functions given in Eq. (18). Keeping ϕ fixed, we obtain the functions c_1,c_2 by the following:

$$c_1=\frac{\iint G_\sigma(x-y)I(y)K(I(y),c_1)H(\phi(x))\mathrm{d}y\mathrm{d}x}{\iint G_\sigma(x-y)K(I(y),c_1)H(\phi(x))\mathrm{d}y\mathrm{d}x} \tag{21}$$

$$c_2=\frac{\iint G_\sigma(x-y)I(y)K(I(y),c_2)(1-H(\phi(x)))\mathrm{d}y\mathrm{d}x}{\iint G_\sigma(x-y)K(I(y),c_2)(1-H(\phi(x)))\mathrm{d}y\mathrm{d}x} \tag{22}$$

With the intuitive explanation obtained from Eqs. (21) and (22), the proposed model has robustness to both noise and outliers. It is evident that we use the kernel function $K(I(y),c_i)$ to determine the degree of similarity between the average intensity c_i and the intensity $I(y)$ in a neighborhood. When $I(y)$ is from noise or outliers, the distance from a point of intensity to the average intensity is very far, so the value of the kernel function will be small, and therefore the influence exerted by $I(y)$ in updating c_1 and c_2 can be suppressed by the additional weight $K(I(y),c_i)$.

In this paper, the size of the kernel function is an important parameter in the image segmentation result. As proposed by the authors in Refs. [17, 18], one way to estimate parameter σ_k is to utilize the distance standard deviation from the image intensities. The distance standard deviation can be used to automatically adjust parameters according to the degree of polymerization of the gray value in different regions, which we define as follows: we assume that the number of pixels in an image is N, and the mean intensity of the whole image is as follows:

$$\overline{I_0}=\frac{\sum_{i=1}^{N}I_0(x_i)}{N} \tag{23}$$

We compute the absolute distance between $I_0(x_i)$ and I_0, which is defined as $d_i=|I_0(x_i)-\bar{I_0}|$. So, the average value of d_i can be expressed by Eq. (24).

$$\overline{d}=\frac{\sum_{i=1}^{N}d_i}{N} \tag{24}$$

Thus, we can define the size parameter σ_k based on the distance standard deviation as follows:

$$\sigma_k=\left(\frac{\sum_{i=1}^{N}(d_i-d)^2}{N-1}\right)^{\frac{1}{2}} \tag{25}$$

3.3 Convex optimization of the energy functional

The energy functional in Eq. (15), as represented by the level set function, is non-convex, so it can easily fall into a local minimum. Chan and Nikolova proposed a

global convex segmentation method[19], which we adopt in our proposed model to reconstruct the corresponding expression. With loss of generality, we introduce a new parameter η and set $\upsilon = 1$, so Eq. (20) can be rewritten as follows:

$$\frac{\partial \phi}{\partial t} = -\delta_{\varepsilon}(\phi)\eta(e_1 - e_2) + \delta_{\varepsilon}(\phi) div\left(\frac{\nabla \phi}{|\nabla \phi|}\right) \tag{26}$$

Using the global convex segment method, the stable solutions of Eq. (26) and Eq. (27) are equivalent.

$$\frac{\partial \phi}{\partial t} = -\eta(e_1 - e_2) + div\left(\frac{\nabla \phi}{|\nabla \phi|}\right) \tag{27}$$

The above simplified flow represents the gradient descent for minimizing the energy:

$$E(\phi) = \int |\nabla(\phi(x))| \mathrm{d}x + \int \phi(x) s(x) \mathrm{d}x \tag{28}$$

where

$$s(x) = e_1 - e_2 \tag{29}$$

To obtain the global minimum, we constrain the level set function ϕ to fall within a finite interval $[a, b]$, so we can obtain the global minimum, as follows:

$$\min_{\phi \in [a,b]} E(\phi) = \min_{\phi \in [a,b]} (|\nabla \phi|_1 + \langle \phi, s \rangle) \tag{30}$$

where $\langle \phi, s \rangle = \int \phi(x) s(x) \mathrm{d}x$. When we obtain the optimum solution ϕ, we can truncate the level set function by a threshold value to obtain the segmentation results[20]:

$$\Omega_1 = \{x : \phi(x) > \alpha\}, \alpha \in (a, b) \tag{31}$$

where α is the threshold value. In this paper, we choose $\alpha = \frac{a+b}{2}$. To utilize edge information, we introduce a weighted Total-Variation (TV) norm, as proposed by the authors in Ref. [21], to replace the standard TV norm:

$$TV_g(\phi) = \int g|\nabla \phi| = |\nabla \phi|_g \tag{32}$$

where g is a nonnegative edge indicator function, which is usually defined as follows:

$$g(\xi) = \frac{1}{1 + \beta |\xi|^2} \tag{33}$$

where β is a constant used to determine the level of detail in the segmentation. Thus, we obtain the following minimization problem:

$$\min_{\phi \in [a,b]} E(\phi) = \min_{\phi \in [a,b]} (|\nabla \phi|_g + \langle \phi, s \rangle) \tag{34}$$

3.4 Split Bregman method for energy minimization

We utilize the split Bregman method[22] to effectively minimize the proposed energy functional. First, we introduce an auxiliary variable d and then use a quadratic penalty term, $\vec{d} = \nabla \phi$, to strengthen this constraint, thereby obtaining the following unconstrained optimization problem:

$$(\phi^*, \vec{d}^*) = \arg \min_{\phi \in [a,b]} \left(|\vec{d}|_g + \langle \phi, s \rangle + \frac{\lambda}{2} \|\vec{d} - \nabla \phi\|^2 \right) \tag{35}$$

where λ is a positive constant. Then, we use Bregman iteration to strictly enforce the constraint $\vec{d} = \nabla \phi$, which yields the following optimization problem:

$$(\phi^{t+1}, \vec{d}^{t+1}) = \arg \min_{\phi \in [a,b]} \left(|\vec{d}|_g + \langle \phi, s \rangle + \frac{\lambda}{2} \|\vec{d} - \nabla \phi - \vec{b}^t\|^2 \right) \tag{36}$$

$$\vec{b}^{t+1} = \vec{b}^t + \nabla \phi^{t+1} - \vec{d}^{t+1} \tag{37}$$

By the calculus of variations and keeping $\vec{d}$ fixed, we obtain the Euler-Lagrange equation about ϕ for the optimization problem Eq. (36), as follows:

$$\triangle \phi = \frac{r}{\lambda} + \nabla \cdot (\vec{d} - \vec{b}), \quad a_0 < \phi < b_0 \tag{38}$$

We adopt the central difference and backward difference schemes for the Laplace operator $\triangle$ and divergence operators ∇, respectively. We then obtain the solution to Eq. (38), as follows:

$$\begin{cases} a_{i,j} = d^x_{i-1,j} - d^x_{i,j} + d^y_{i,j-1} - d^y_{i,j} - \\ (b^x_{i-1,j} - b^x_{i,j} + b^y_{i,j-1} - b^y_{i,j}), \\ \beta_{i,j} = \frac{1}{4}\left(\phi_{i-1,j} + \phi_{i+1,j} + \phi_{i,j-1} + \phi_{i,j+1} - \frac{s}{\lambda} + a_{i,j}\right), \\ \phi_{i,j} = \max\{\min\{\beta_{i,j}, b\}, a\} \end{cases} \tag{39}$$

Keeping ϕ fixed and minimizing Eq. (36) with respect to $\vec{d}$, we obtain the following:

$$\vec{d}^{t+1} = shrink_g(\vec{b}^t + \nabla \phi^{t+1}, \frac{1}{\lambda}) = shrink(\vec{b}^t + \nabla \phi^{t+1}, \frac{g}{\lambda}) \tag{40}$$

where

$$shrink(x, \lambda) = \frac{x}{|x|} \max(|x| - \lambda, 0) \tag{41}$$

In summary, the algorithm implementation steps are as follows:

Step 1: Initialize the level set function ϕ and calculate the initial values of c_1^0 and c_2^0.

Step 2: Update c_1 and c_2 using Eqs. (21) and (22).

Step 3: Update s using Eq. (29).

Step 4: Update ϕ using Eq. (39).

Step 5: Update $\vec{d}$ using Eq. (40).

Step 6: Update $\vec{b}$ using Eq. (37).

Step 7: $\Omega = \{x : \phi(x) > \alpha\}$.

Step 8: Check whether the evolution has converged. If not, return to Step 2.

In this paper, we simply initialize the level set function as a binary function, and choose $a = 2$ inside the contour and $b = -2$ outside the contour. Then, we can choose a threshold $\frac{a+b}{2}$ for α to identify segmented regions. Experimental results have shown this simple initialization to be effective[19].

4 Experimental Results

In this section, we demonstrate the robustness and effectiveness of our proposed method based on the results of experiments we conducted on synthetic images, medical images, and the Berkeley Segmentation Dataset. We compare the results of our method with four representative methods, including the CV, RSF, recursive least squares method RLSM, and LIC models. We implemented the proposed model using Matlab2012a on a computer with a Pentium CPU 2.50, 4 GB of RAM, and the Windows 7 operating system. Without other specifications, we used the following default parameter settings in the experiments: $\eta = 10$, $\lambda = 0.01$, $\beta = 255 \times 255$, with which our model achieved satisfactory segmentation results on different types of images. We plotted the initial and final contours in blue and red, respectively, for all the experiments.

To quantitatively compare our proposed model with other active contour models, we used two metrics to access the segmentation results: the Dice Similarity Coefficient (DSC)[23, 24] and the Jaccard Similarity (JS)[24, 25], respectively, which are defined as follows:

$$\mathrm{DSC} = \frac{2 \cdot N(S_1 \bigcap S_2)}{N(S_1) + N(S_2)}, \quad \mathrm{JS} = \frac{N(S_1 \bigcap S_2)}{N(S_1 \bigcup S_2)} \tag{42}$$

where $N(\bullet)$ represents the pixel numbers in the enclosed set, and S_1 and S_2 indicate the segmentation results obtained by ground truth and the proposed model, respectively. The closer are the DSC and JS values to 1, the better are the segmentation results.

4.1 Experiments on images with intensity inhomogeneity

To demonstrate the efficiency of the proposed model, we conducted experiments on three different images with intensity inhomogeneity, the results of which are shown in Fig. 1. These images included one of a cell with blurred boundaries and some cells very close to each other, a synthetic image with different shapes and an interior hole, and a noisy image. The original images and initial contours are shown in Figs. 1a, 1c, and 1e, and the corresponding segmentation results are shown in Figs. 1b, 1d, and 1f. We chose the parameter $\sigma = 3$ for all three images in this

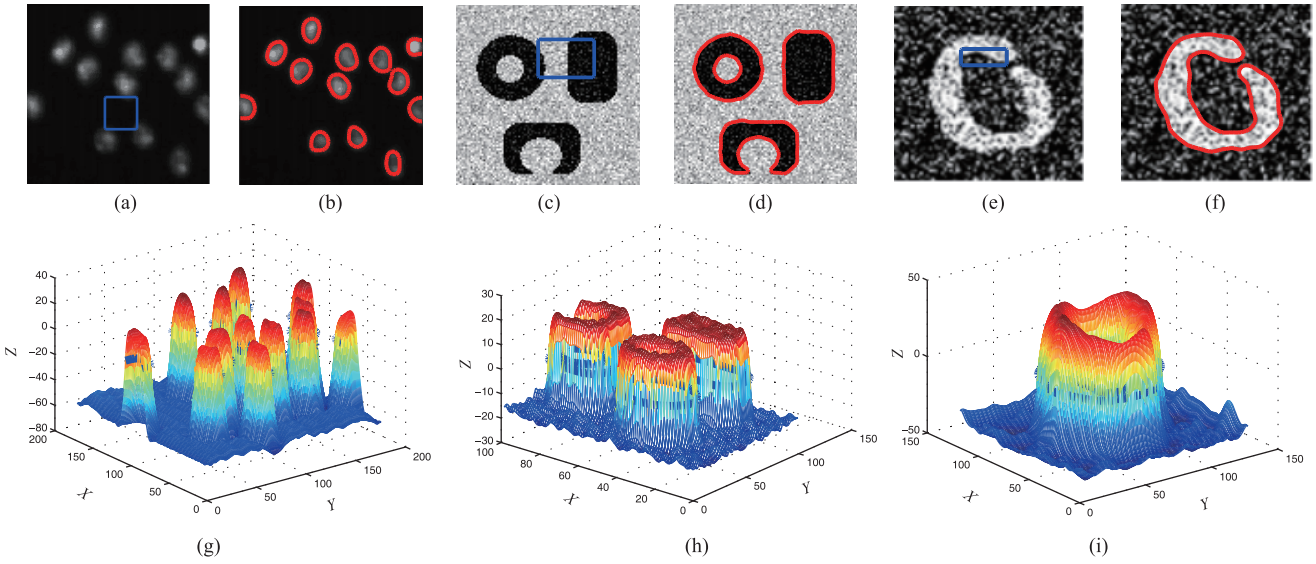

Fig. 1 Segmentation results using our proposed model for a medical image, a synthetic image with blurred boundaries, and a noisy synthetic image. (a, c, e) Original images with initial contour. (b, d, f) Segmentation results. (g, h, i) Corresponding final level set functions with the zero level set in solid blue line.

experiment. The successful segmentation of all the images indicates that our method is robust with respect to blurred object boundaries and noise. By introducing local information and a kernel distance metric into the proposed model, the influence of noise and outliers can be suppressed. Figures 1g, 1h, and 1i show the corresponding final level set functions.

4.2 Robustness to contour initialization and parameter σ

To evaluate the proposed model's robustness to contour initialization, we applied it to a real image with 15 different initializations. Figure 2 shows five of the 15 initial contours and the final segmentation results. In this experiment, we set parameter $\sigma = 3$. As we can see in the figure, the initial contours with different shapes are located in different regions, i.e., outside, inside, and across the object. Despite the significant differences between these initial contours, the corresponding results are very similar, and the object boundaries have been accurately captured. We quantitatively evaluated the segmentation accuracy by considering these results in terms of their JS and DSC values. As shown in Fig. 3, the JS and DSC values of these results are all above 0.9401, which demonstrates the robustness of our model to the initial contour.

We also used different scales for parameter σ, which is a critical parameter in the algorithm, to test the performance of our proposed model. We applied seven different values of σ in an image, from 2 to 8. Increasing the value of parameter σ can introduce more local intensity information to the model, but a large σ value can lead to the over-smoothing of a noisy image, wherein even the boundaries of the object can become blurred. We computed the JS and DSC values for these seven results, which are plotted in Fig. 4. As we can see in the figure, with increases in σ, the segmentation accuracy is significantly improved when $\sigma \leqslant 3$ and gradually decreases when $\sigma > 3$. However, the JS and DSC values are all greater than 0.9 when the parameter ranges from 2 to 7. This experiment demonstrates the robustness of our model to parameter σ within a certain range.

4.3 Comparison with CV model, RSF model, RLSM model

In this section, we compare our results with those of three

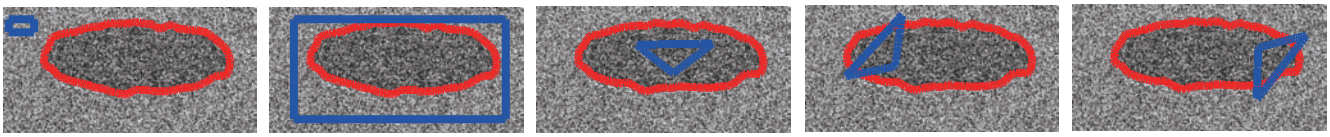

(a) (b) (c) (d) (e)

Fig. 2 Results of our model with different initial contours on a natural image. The initial and final contours are plotted in blue and red, respectively.

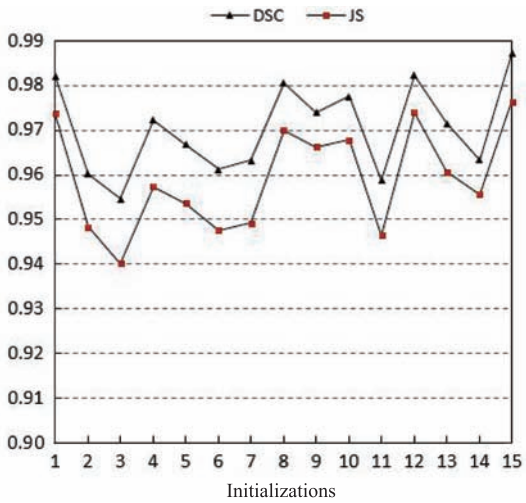

Fig. 3 DSC and JS values of the results for 15 different initializations.

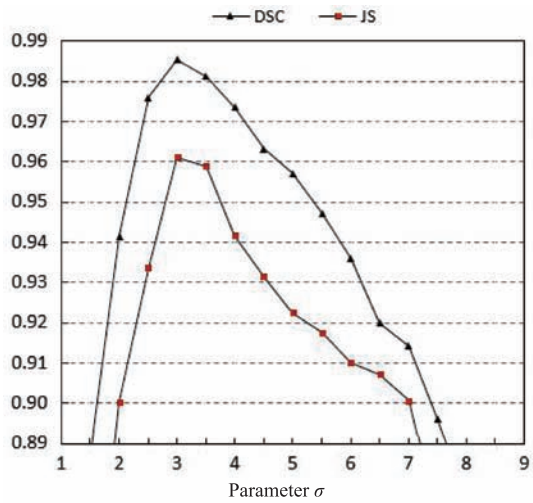

Fig. 4 DSC and JS values for different scale parameters σ.

typical models known as the CV, RSF, and RLSM models. As shown in Fig. 5, we tested our method on two real images from the Berkeley Segmentation[26]. In the experiment, we used the same initial contours for the four models. The segmentation results of the CV, RSF, RLSM and proposed models are presented in the second to the fifth columns in Fig. 5, respectively. To obtain more detailed object information, we set parameters $\sigma = 3$ and $\sigma = 4$. In the figure, we can see that the segmentation results of the CV, RSF, and RLSM models are not accurate. This is because these models use Euclidean distance to measure the distance between pixels and the fitting center. As shown in the last column of Fig. 5, our method successfully extracted the object boundaries. We attribute the success of this result to our utilization of the robust kernel distance metric.

4.4 Performance with noisy images

In the next three experiments, we tested the effectiveness of the proposed method on images with various noise levels. Figure 6 shows a comparison of the results of our method with those of the RSF, LIC, and RLSM models on an infrared image. As we can see in the first row of the figure, the input image is polluted by salt-and-pepper noise with noise density levels (from left to right) of 0.05, 0.1, 0.2, 0.4, 0.6, and 0.8, respectively. The segmentation results of the RSF, LIC, and RLSM models are shown in the second, third, and fourth rows of Fig. 6, respectively. From left to right, we chose the parameters $\sigma = 2$, $\sigma = 2$, $\sigma = 3$, $\sigma = 3$, $\sigma = 4$, and $\sigma = 4$, respectively, in our experiment. In the figure, we can see that when the noise density is $\leqslant 0.2$, all the models can accurately capture the object, but when the noise density is greater than 0.2, the RSF and LIC models cannot obtain accurate results. The RLSM model works well on images with salt-and-pepper noise, but as the noise density increases >0.2, its segmentation results become worse, and the model wrongly classifies the background as the object. In contrast, we can see from the last row of Fig. 6 that our model obtained satisfactory segmentation results for the challenging noisy images. Table 1 lists the CPU time and number of iterations for segmentation, in which we can see that the number of iterations and CPU time of the proposed model are significantly less than those of the other three models, due to the introduction of the split Bregman method. These experimental results show that our model effectively suppresses the effect of salt-and-pepper noise to achieve an exact and robust segmentation result.

In Fig. 7, we compare our model results with those of two classical active contour models—the RSF and LIC models—on a real image with various Gaussian noise levels. In the first row of Fig. 7 (from left to right), the image had a Gaussian noise level mean of 0.2 and variance 0.05, mean 0.2 and variance 0.1, mean 0.4 and variance 0.2, mean 0.4 and variance 0.4, mean 0.6 and variance 0.6, and mean 0.8 and variance 0.8, respectively. In this experiment (from left to right), we set the parameter $\sigma = 3$, $\sigma = 3$, $\sigma = 4$, $\sigma = 4$, $\sigma = 4$, and $\sigma = 5$, respectively. The segmentation results for the RSF, LIC, and proposed models are shown in the second, third, and last rows of Fig. 7, respectively, in which we can see that the RSF model failed to segment the objects disturbed by Gaussian noise because it draws only upon the intensity means in local regions during the segmentation process. When the

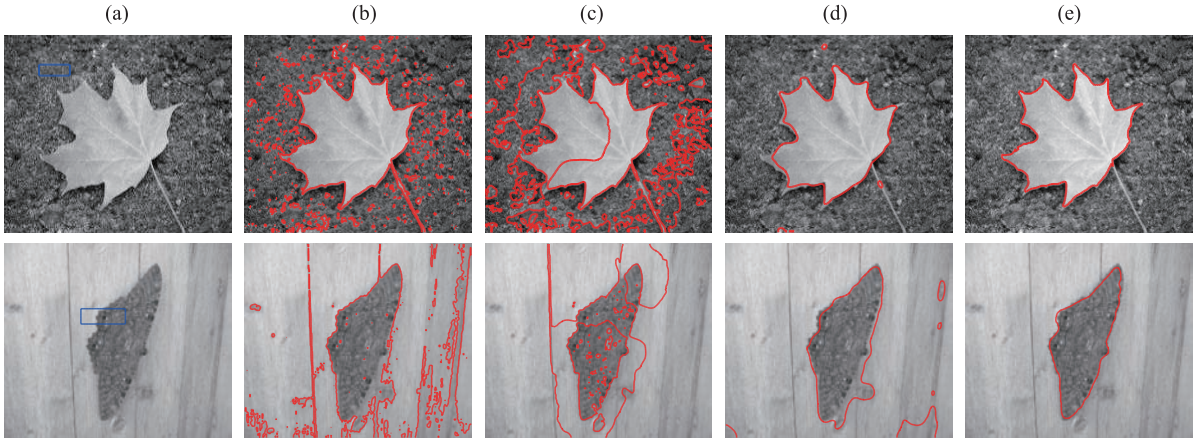

Fig. 5 Comparison of our method with the CV, RSF, and RLSM models for two real images. (a) Original images with initial contours. (b) Segmentation results of the CV model. (c) Segmentation results of the RSF model. (d) Segmentation results of the RLSM model. (e) Segmentation results of the proposed model.

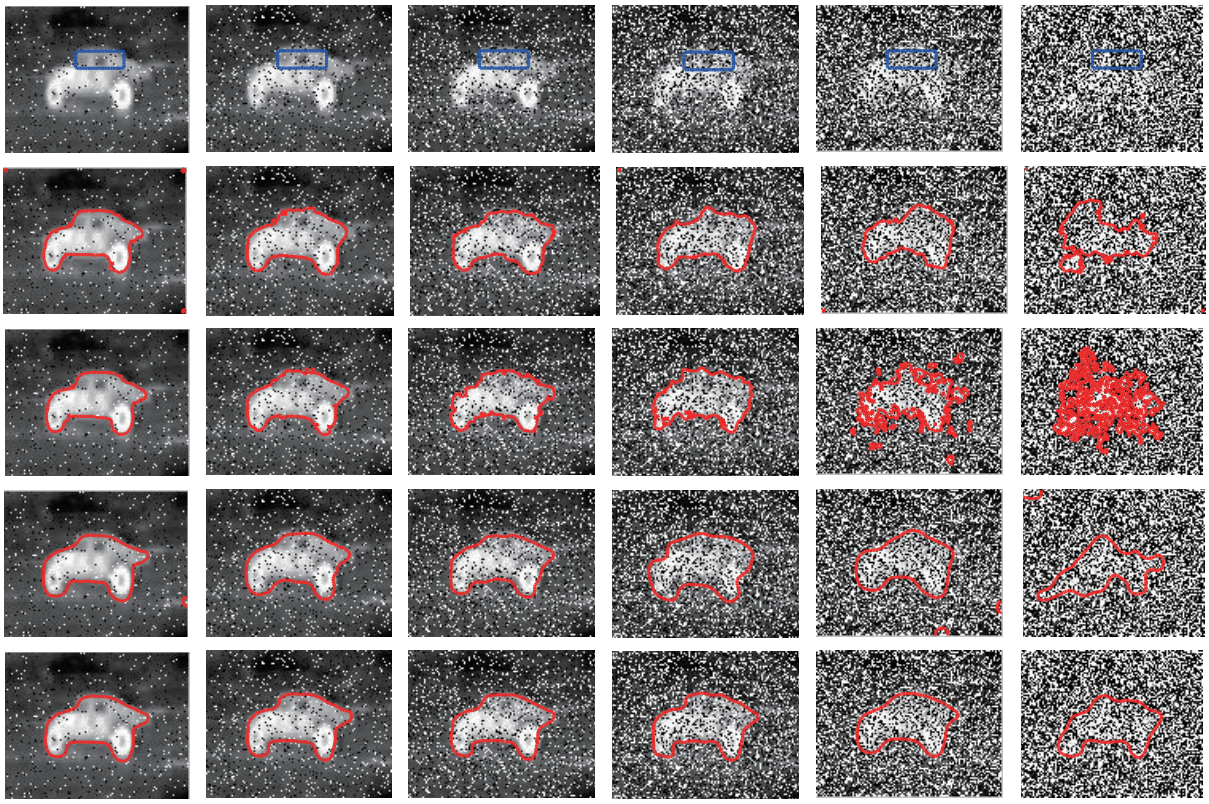

Fig. 6 Segmentation results for an infrared image with various levels of salt-and-pepper noise. First to sixth columns show noise density levels of 0.05, 0.1, 0.2, 0.4, 0.6, and 0.8, respectively. First row: Original images with initial contours. Second row: RSF model results. Third row: LIC model results. Fourth row: RLSM model results. Fifth row: Proposed model results.

Table 1 Number of iterations and CPU times for RSF, LIC, RLSM models, and our proposed method for the results shown in Fig. 6.

	RSF model		LIC model		RLSM model		Our method	
	Iterations	Time (s)	Iterations	Time (s)	Iterations	Time (s)	Iterations	Time (s)
Column 1	60	3.524 999	250	2.368 718	80	2.010 718	2	0.262 261
Column 2	60	3.789 980	200	2.067 538	100	2.401 176	1	0.262 959
Column 3	70	4.279 330	200	2.064 577	130	2.660 697	3	0.279 622
Column 4	100	5.862 987	250	3.009 85	150	2.724 729	3	0.278 509
Column 5	100	6.170 390	300	3.533 86	150	2.823 181	3	0.281 412
Column 6	120	10.723 534	300	3.853 397	150	2.879 318	3	0.285 208

variance of the Gaussian noise is low (< 0.4), the LIC model can effectively segment the boundary of an object. However, when the variance reaches 0.4 ($\geqslant 0.4$), the LIC model cannot obtain satisfactory segmentation results. When the variance values are 0.6 and 0.8, the object and background are very similar in the images, but with the help of the robust kernel distance metric, our model can accurately distinguish between the background and foreground. From these results, we can see that the RSF and LIC models, which use the Euclidean distance as the sole criterion for classification, cannot correctly detect the object boundary. This experiment demonstrates that our proposed model has better robustness to Gaussian noise than the other two active contour models.

In the last experiment, we tested for model robustness to speckle noise with different variances, and compared our model results with those of the LIC and RLSM models, as shown in Fig. 8. In the first row of the figure, the infrared image has been contaminated by speckle noise at variances of 0.01, 0.05, 0.1, 02, 0.3, and 0.4, respectively, from left to right. The corresponding results of the LIC, RLSM,

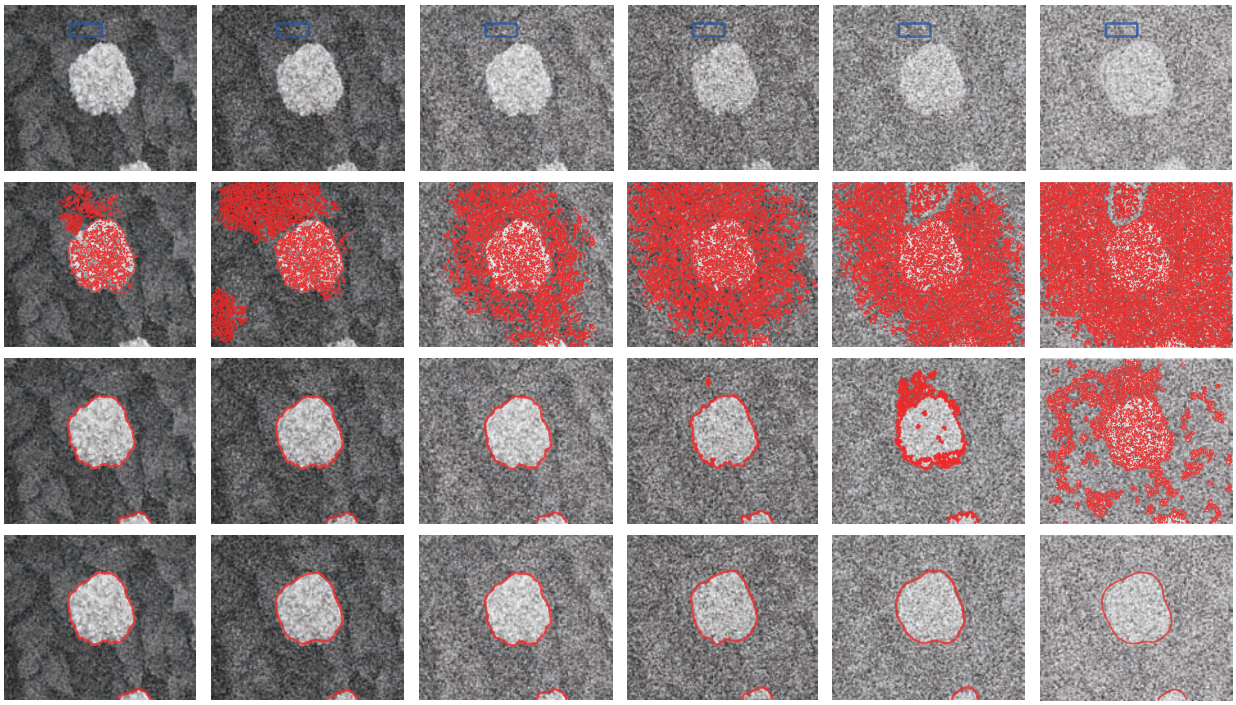

Fig. 7 Segmentation results of a real image with various levels of Gaussian noise. First to sixth columns show Gaussian noise levels with a mean of 0.2 and variance of 0.05, mean 0.2 and variance 0.1, mean 0.4 and variance 0.2, mean 0.4 and variance 0.4, mean 0.6 and variance 0.6, and mean 0.8 and variance 0.8, respectively. First row: Original images with initial contours. Second row: RSF model results. Third row: LIC model results. Fourth row: Proposed model results.

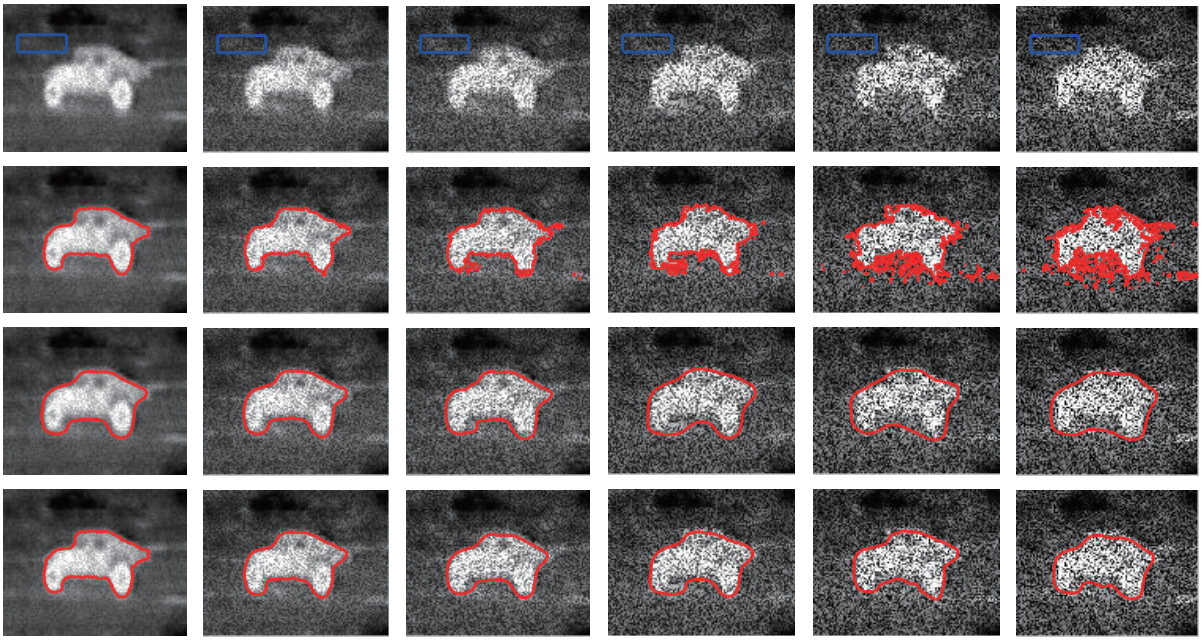

Fig. 8 Segmentation results for an infrared image with various levels of speckle noise. The first to sixth columns have added speckle noise with variances of 0.01, 0.05, 0.1, 0.2, 0.3, and 0.4, respectively. First row: Original images with initial contours. Second row: LIC model results. Third row: RLSM model results. Fourth row: Proposed model results.

and proposed models are shown in the second, third, and last rows, respectively. In the experiment, we set parameters $\sigma = 3$, $\sigma = 3$, $\sigma = 3$, $\sigma = 4$, $\sigma = 4$, and $\sigma = 4$, respectively, from left to right. From these segmentation results, we can see that the LIC model can obtain accurate segmentation results when the variance is $\leqslant 0.05$. However, the segmentation results become worse with increasing variance > 0.05. By a visual evaluation of the last two rows of Fig. 8, we can see that the segmentation results of the RLSM model appear similar to those of the proposed model. To quantitatively evaluate the robustness of our method, we used the metrics described above. We computed the DSC and JS values of the three models for the infrared image polluted by speckle noise, which are listed in Table 2. From the table, we can see that our model draws upon the local intensity information and, with the kernel distance metric, achieves more accurate segmentation results. Moreover, compared with the other two models, the proposed model is more robust to speckle noise.

5 Conclusion

In this paper, we presented a new active contour model in which local information is introduced into the CV model and kernel function metrics are used to create a nonlinear energy functional. This model can overcome the problems associated with sensitivity to noise and singular values, thereby improving the accuracy of image segmentation. To reduce the dependence on the location of the initial curve, we use a convex optimization of the level set. In addition, we use the split Bregman iteration method to obtain a numerical solution, thus improving the accuracy and efficiency of segmentation. Our experimental results demonstrate the good performance of our method for images with intensity inhomogeneity. Compared to other models, our proposed model demonstrates more robustness to various noise, as well as advantages in terms of efficiency and accuracy.

Table 2 DSC and JS values for the results shown in Fig. 8.

	LIC model		RLSM model		Our model	
	DSC	JS	DSC	JS	DSC	JS
Column 1	0.9956	0.9912	0.9623	0.9576	0.9963	0.9947
Column 2	0.9438	0.9323	0.9563	0.9479	0.9815	0.9799
Column 3	0.8784	0.8523	0.9317	0.9221	0.9528	0.9467
Column 4	0.7938	0.7673	0.8845	0.8652	0.9206	0.9029
Column 5	0.6654	0.6449	0.8527	0.8315	0.9031	0.8926
Column 6	0.5917	0.5702	0.8046	0.7896	0.8912	0.8742

Acknowledgment

This study was supported by the National Natural Science Foundation of China (No. 61472270).

References

[1] X. Liu, X. Tao, and N. Ge, Fast remote-sensing image registration using priori information and robust feature extraction, *Tsinghua Science and Technology*, vol. 21, no. 5, pp. 552–560, 2016.

[2] J. Liu, M. Li, J. Wang, F. Wu, T. Liu, and Y. Pan, A survey of MRI-based brain tumor segmentation methods, *Tsinghua Science and Technology*, vol. 19, no. 6, pp. 578–595, 2014.

[3] M. Kass, A. Witkin, and D. Terzopolos, Snakes: Active contour models, *International Journal of Computer Vision*, vol. 1, no. 4, pp. 321–331, 1988.

[4] V. Caselles, R. Kimmlel, and G.Sapiro, Geodesic active contours, *International Journal of Computer Vision*, vol. 22, no. 1, pp. 61–79, 1997.

[5] C. Li, C. Xu, C. Gui, and M. D. Fo, Level set evolution without re-initialization: A new variational formulation, in *Proceedings of IEEE Conference on Computer Vision and Pattern Recognition*, San Diego, CA, USA, 2005, pp. 430–436.

[6] A. Vasilevskiy and K. Siddiqi, Flux maximizing geometric flows, *IEEE Transactions on Pattern Analysis and Machine Intelligence*, vol. 24, no. 12, pp. 1565–1578, 2002.

[7] L. Fang and X. Wang, Image segmentation frame work using edgeflow-based active contours, *Optik*, vol. 124, no. 18, pp. 3739–3745, 2013.

[8] D. Mumford and J. Shah, Optimal approximation by piecewise smooth functions and associated variational problems, *Communications on Pure and Applied Mathematics*, vol. 42, no. 5, pp. 577–685, 1989.

[9] T. Chan and L. Vese, Active contours without edges, *IEEE Transaction on Image Processing*, vol. 10, no. 2, pp. 266–277, 2001.

[10] C. Li, C. Kao, J. C. Gore, and Z. Ding, Minimization of region-scalable fitting energy for image segmentation, *IEEE Transactions on Image Processing*, vol. 17, no. 10, pp. 1940–1949, 2008.

[11] K. Zhang, H. Song, and L. Zhang, Active contours driven by local image fitting energy, *Pattern Recognition*, vol. 43, no. 4, pp. 1199–1206, 2010.

[12] C. Li, R. Huang, Z. Ding, and J. C. Gatenby, A level set method for image segmentation in the presence of intensity inhomogeneities with application to MRI, *IEEE Transactions on Image Processing*, vol. 20, no. 7, pp. 2007–2016, 2011.

[13] L. Wang, L. He, A. Mishra, and C Li, Active contours driven by local Gaussian distribution fitting energy, *Signal Processing*, vol. 89, no. 12, pp. 2435–2447, 2009.

[14] S. Liu and Y. Peng, A local region-based Chan-Vese model for image segmentation, *Pattern Recognition*, vol. 45, no. 7, pp. 2769–2779, 2012.

[15] X. Xie, C. Wang, A. Zhang, and X. Meng, A robust level set method based on local statistical information for noisy image segmentation, *Optik*, vol. 125, no. 9, pp. 2199–2204, 2014.

[16] P. V. Gehler, An introduction to kernel-based learning algorithms, *IEEE Transactions on Neural Networks*, vol. 12, no. 2, pp. 181–201, 2001.

[17] M. Gong, Y. Liang, and J. Shi, Fuzzy C-means clustering with local information and kernel metric for image segmentation, *IEEE Transactions on Image Processing*, vol. 22, no. 2, pp. 573–584, 2012.

[18] Y. Wu, W. Ma, and M. Gong, Novel fuzzy active contour model with kernel metric for imagesegmentation, *Applied Soft Computing*, vol. 34, pp. 301–311, 2015.

[19] T. Chan and M. Nikolova, Algorithms for finding global minimizers of image segmentation and denoising models, *SIAM Journal on Applied Mathematics*, vol. 66, no. 5, pp. 1632–1648, 2006.

[20] Y. Yang and B. Wu, Split Bregman method for minimization of improved active contour model combining local and global information dynamically, *Journal of Mathematical Analysis and Applications*, vol. 389, no. 1, pp. 351–366, 2013.

[21] X. Bresson, S. Esedoglu, and P. Vandergheynst, Fast global minimization of the active contour/snake model, *Journal of Mathematical Imaging and Vision*, vol. 28, no. 2, pp. 151–167, 2007.

[22] T. Goldstein, X. Bresson, and S. Osher, Geometric applications of the split Bregman method: Segmentation and surface reconstruction, *Journal of Scientific Computing*, vol. 45, no. 1, pp. 272–293, 2010.

[23] L. Wang, C. Li, and Q. Sun, Active contours driven by local and global intensity fitting energy with application to brain MR image segmentation, *Computerized Medical Imaging and Graphics*, vol. 33, no. 7, pp. 520–531, 2009.

[24] U. Vovk, A review of methods for correction of intensity inhomogeneity in MRI, *IEEE Transactions on Medical Imaging*, vol. 26, no. 3, pp. 405–421, 2007.

[25] Q. Zheng, Z. Lu, Y. Wei, and M Zhang, A robust medical image segmentation method using KL distance and local neighborhood information, *Computers in Biology and Medicine*, vol. 43, no. 5, pp. 459–470, 2013.

[26] D. Martin, C. Fowlkes, and D. Tal, A database of human segmented natural images and its application to evaluating segmentation algorithms and measuring ecological statistics, *IEEE International Conference on Computer Vision*, vol. 2, no. 11, pp. 416–423, 2002.

Gang Li is currently a PhD student at Taiyuan University of Technology, China. His principal research interest is image processing and intelligent information processing, etc.

Ling Zhang is a lecturer at Taiyuan University of Technology. She received the PhD degree from Taiyuan University of Technology in 2016. She is a senior member of CCF. Her principal research interest is image processing and visual information processing, etc.

Haifang Li is a professor and doctoral supervisor at Taiyuan University of Technology, China. She served as deputy secretary general of the computer in Shanxi Province. She has been engaged in parallel and distributed technology, image processing, emotional computing, and brain informatics research and has get a number of achievements. She has hosted and completed three research programs of the National Natural Science Foundation of China, more than ten provincial projects, and some other transverse projects.